Energy and Climate

Enhancement of the generation and transfer of active oxygen in Ni/CeO2 catalysts for soot combustion by controlling the Ni-ceria contact and the three-dimensional structure

Begoña Sellers-Antón, Esther Bailon-Garcia, Andrea Cárdenas-Arenas, Arantxa Davó-Quiñonero, Dolores Lozano-Castello, and Agustín Bueno-López

Environ. Sci. Technol., **Just Accepted Manuscript** • DOI: 10.1021/acs.est.9b07682 • Publication Date (Web): 16 Jan 2020

Enhancement of the generation and transfer of active oxygen in Ni/CeO_2 catalysts for soot combustion by controlling the Ni-ceria contact and the three-dimensional structure

Begoña Sellers-Antón, Esther Bailón-García, Andrea Cardenas-Arenas, Arantxa Davó-Quiñonero, Dolores Lozano-Castelló and Agustín Bueno-López*

Department of Inorganic Chemistry, University of Alicante, Carretera de San Vicente s/n. E03080, Alicante (Spain).

*Corresponding Author: Esther Bailón-García

Email: estherbg@ugr.es

Keywords: soot, nickel, ceria, 3DOM, NO_x

Abstract

The effect of the 3DOM structure and the Ni-doping of CeO_2 on the physicochemical properties and catalytic activity for the soot combustion was studied. Moreover, the way in which Ni is introduced to the ceria support was also investigated. For that, CeO_2 supports were synthesised with uncontrolled (Ref) and 3DOM structured morphology and their respective Ni/CeO_2 catalysts were prepared by impregnation of the previously synthesised supports or by successive impregnation of both precursors (Ni and Ce) on the 3DOM template. Conclusions reached in this study are: (1) the 3DOM structure increases the surface area of the catalysts and improves the catalyst-soot contact. (2) The doping of CeO_2 with Ni improves the catalytic activity because the NiO participates in the catalytic oxidation of NO to NO_2, and also favours the production of active oxygen and the catalyst oxygen storage capacity. (3) Ni incorporation method affects its physicochemical and catalytic properties. By introducing the Ni by successive infiltration in the solid template, the CeO_2 crystals size is reduced, Ni dispersion is improved, and the catalyst reducibility is increased. All these characteristics make the catalyst synthesized by successive infiltration to have a catalytic activity for the soot combustion higher than the Ni-impregnated CeO_2 catalyst.

1. INTRODUCTION

CeO_2 is widely used as oxidation catalyst owing to its ability to provide highly reactive active oxygen as a consequence of its ability to undergo rapid redox cycles.[1] Consequently, ceria-based catalysts are presented as one essential component of high-performance three-way catalyst (TWC) for the removal of diesel engines exhaust pollutants such as NO_x, hydrocarbons, and particulate matter.[2]

Despite the high activity of ceria as oxidation catalyst, a loss of the ceria oxygen storage capacity is observed at high temperature, with the consequent loss of activity, due to the sintering of ceria particles and grain growth.[3] Therefore, the development of advanced catalysts with improved thermal resistance to the sintering and higher oxygen storage capacity is required and widely researched worldwide. The oxygen storage capacity, the surface reducibility and the thermal stability can be improved by doping ceria with proper foreign cations.[4,5]

Different heteroatoms have been used to dope ceria in order to modify its chemical properties and enhance the catalytic activity and thermal stability, such as Zr and rare-earth metals (La and Pr),[6–12] transition metals (Cu, Co, Mn, Cr and Fe),[4,13–16] alkali and alkali-earth metals (K, Cs, Na, Ca, Ba and Mg)[17,18] and noble metals (Ag, Au, Pd, Ru and Rh)[19,20] obtaining materials with better oxidative performance. Liu Shuang *et al*.[4] have analysed the catalytic behaviour in the soot combustion of different doped ceria systems described in the recent literature and they concluded that the soot oxidation activity of catalysts generally follows the order: alkali metals- > transition metals- ≥ noble metals-

> Zr and rare-earth metals-doped CeO_2 in both O_2 and $NO+O_2$ catalytic conditions. However, alkali metals-modified ceria catalysts are, usually, thermally unstable due to the volatile nature of the alkali metal species [17] and noble metals-modified ceria catalysts are cost-prohibitive. Thus, it seems that the transition metals and rare earth metals, especially $Ce_xZr_{1-x}O_2$ are the best option in terms of activity, thermal stability and cost-efficiency.[21,22]

Nonetheless, in the design of soot combustion catalysts, the contact area between the catalyst and soot particles determines the catalytic efficiency. Common ceria-based catalysts present a low surface area and narrow pore size distribution[23] and therefore, a restricted number of active sites due to the limited soot–catalyst points of contact. Thus, together with the improvement of the generation of active oxygen, the solid-solid contact must be also taken into account in the design of soot combustion catalyst to ensure the transfer of that active oxygen. In that sense, three-dimensionally ordered macroporous (3DOM) materials have acquired great interest in the scientific community.[13,24] These 3DOM materials present a homogeneous and wide pore size distribution which consists of an interconnected structure of pores above 50 nm which favours the diffusion of the soot particles in the inner pores and facilitates the contact between soot and catalyst particles.[25,26]. J. Xiong et al. have demonstrated that the 3DOM structure increases the amount of supported active sites and enhances the contact efficiency between reactants (soot, O_2, and NO) and catalysts.[21,22] In a similar way, J.Wang et al. attributed the high activity of $CuO–CeO_2$ catalysts to the enlarged contact area between the catalyst and soot particles and the improved mass transfer caused by the well-defined 3DOM structure and the enhanced redox capability at low temperatures mainly associated with the highly dispersed copper species.[27] Thus, 3DOM catalysts greatly improve the catalytic efficiency for soot combustion.[21,22,28,29]

With that background, in the present work $NiO\text{-}CeO_2$ catalysts with 3DOM structure have been prepared in order to improve the active oxygen generation by modification with Ni and the transfer of this active oxygen from the catalyst to the soot particles by the 3DOM structure. Different NiO incorporation method to the 3DOM structure have been studied in order to analyse the influence of the NiO-ceria contact to the generation and transfer of such active oxygen.

2. MATERIALS AND METHODS

2.1. Catalysts preparation

CeO_2 supports were prepared with uncontrolled (Ref) and three dimensionally ordered macroporous (3DOM) structures. CeO_2-Ref was prepared by calcination of a dried ethanolic solution of cerium citrate obtained by dissolving $Ce(NO_3)_3 \cdot 6H_2O$ (Sigma-Aldrich) in ethanol and adding citric acid in stoichiometric proportion (Ce/citric acid molar ratio 1:1). The synthesis of CeO_2-3DOM was described elsewhere.[30] Briefly, polymethylmethacrylate (PMMA) colloidal crystals were synthesized by polymerization of methylmethacrylate, methacrylic acid and divinylbenzene in boiling aqueous solution. Then, an ethanolic solution of cerium citrate was infiltrated in the PMMA crystal template. Finally, the Ref and 3DOM ceria supports were calcined at 600 ºC for 6 hours with a heating rate of 1 ºC/min.

Ni catalysts have been prepared by incipient wetness impregnation of the CeO_2 supports. The appropriate amount of $Ni(NO_3)_2 \cdot 6H_2O$ (Sigma-Aldrich) was dissolved in ethanol and was added to the CeO_2-Ref and CeO_2-3DOM supports. Finally, the catalysts were dried at 80 ºC overnight and treated at 600 ºC in a muffle in static air. These catalysts are referred to as Ni/CeO_2-Ref and Ni/CeO_2-3DOM.

A catalyst referred to as (Ni-Ce)-3DOM was prepared by successive impregnation of nickel and cerium precursors into the PMMA template. The appropriate amount of nickel nitrate was dissolved in ethanol and the stoichiometric amount of citric acid to obtain nickel citrate was added (Ni/citric acid molar ratio 1:4). This ethanolic solution was infiltrated in the PMMA crystal template and dried at 80 ºC overnight. Subsequently, an ethanolic solution of cerium nitrate and citric acid in stoichiometric proportion was infiltrated in the Ni/PMMA sample, dried at 80 ºC overnight and finally calcinated at 600 ºC for 6 hours with a heating rate of 1 ºC/min.

The target Ni loading in all catalysts was 8.5 Wt. %.

2.2. Catalysts characterization

The morphology of the samples was analysed by Field Emission Scanning Electron Microscopy (FESEM) using a Merlin VP Compact microscope from Zeiss, working at very low voltages (from 0.02 kV to 30 kV) to minimize charging effects.

The textural characterization of catalysts was carried out by N_2 adsorption at -196 ºC (Autosorb-6, Quantachrome) and mercury porosimetry (Poremaster 60 GT, Quantachrome). To obtain the N_2 adsorption-desorption isotherms and mercury intrusion profiles, the catalysts were previously outgassed under vacuum at 150 ºC for 2 h and 50 ºC for 12 hours, respectively.

The surface chemistry was characterized by X-ray photoelectron spectroscopy (XPS) in a K-ALPHA Thermo Scientific device, using Al-Kα radiation (1486.6 eV). The X-ray spot was focussed on the catalysts with a diameter of 400 μm, at 3 mA × 12 kV. The binding energy scale was adjusted by setting the C_{1s} transition at 284.6 eV.

Temperature programmed reduction experiments were carried out with H_2 (H_2-TPR) in a thermobalance (Mettler Toledo; TGA/SDTA851) coupled to a mass spectrometer (Pfeiffer Vacuum; Thermostar GSD301T). The catalysts (20 mg) were heated in 5% H_2/Ar (40 ml/min) at 10 ºC/min from room temperature until 900 ºC.

The composition of the catalysts was determined by X-ray microfluorescence in an Obis Micro-XRF Analyzer from EDAX. Areas of 300 μm in diameter were analysed and three different spots were measured and averaged to obtain the composition of each catalyst.

The crystal structure was studied by X-ray diffraction in a Rigaku Miniflex II diffractometer. The diffractograms were recorded in a range of 2θ from 10º to 90º, with a

step of 0.025º. The wavelength used was $\lambda = 0.155418$ nm corresponding to the CuK_α radiation. The average crystal size (D) was determined using the Scherrer equation.[31,32]

2.3. Catalytic tests.

Catalytic experiments at programmed temperature (25–700 °C at 10 °C/min) were carried out in a fixed-bed tubular quartz reactor using a mixture of 20 mg of carbon black (Printex U), 80mg of catalyst and 300 mg SiC, prepared with a spatula in the so-called loose-contact mode in order to obtain results with practical meaning. The gas mixture used (500 ml/min; GHSV=30,000 h^{-1}) was composed of 500 ppm NO and 5% O_2 in N_2 balance. The composition of the exhaust gases was controlled by Specific NDIR-UV gas analyzers for CO, CO_2, NO, NO_2 and O_2 (Fisher–Rosemount, models BINOS 100, 1001 and 1004).

3. RESULTS AND DISCUSSION

3.1. Morphological and textural characterization

Scanning electron microscopy (FESEM) images of the catalysts are shown in **Figure 1.** A three dimensionally ordered macroporous structure is clearly identified for 3DOM samples (**Figure 1 b-d**) whereas a smooth and closed surface is observed for the Ref material (**Figure 1a**). In the 3DOM samples, voids are also observed in the cerium walls (which are circled in **Figure 1d** as an example) generated by the incomplete filling of the interstitial spaces between the PMMA spheres. Thus, a bimodal pore size distribution is obtained with sizes ranging between 60-80 nm and 160-180 nm for the interstitial spaces and macropores generated by the PMMA combustion, respectively (**Figure S1**).

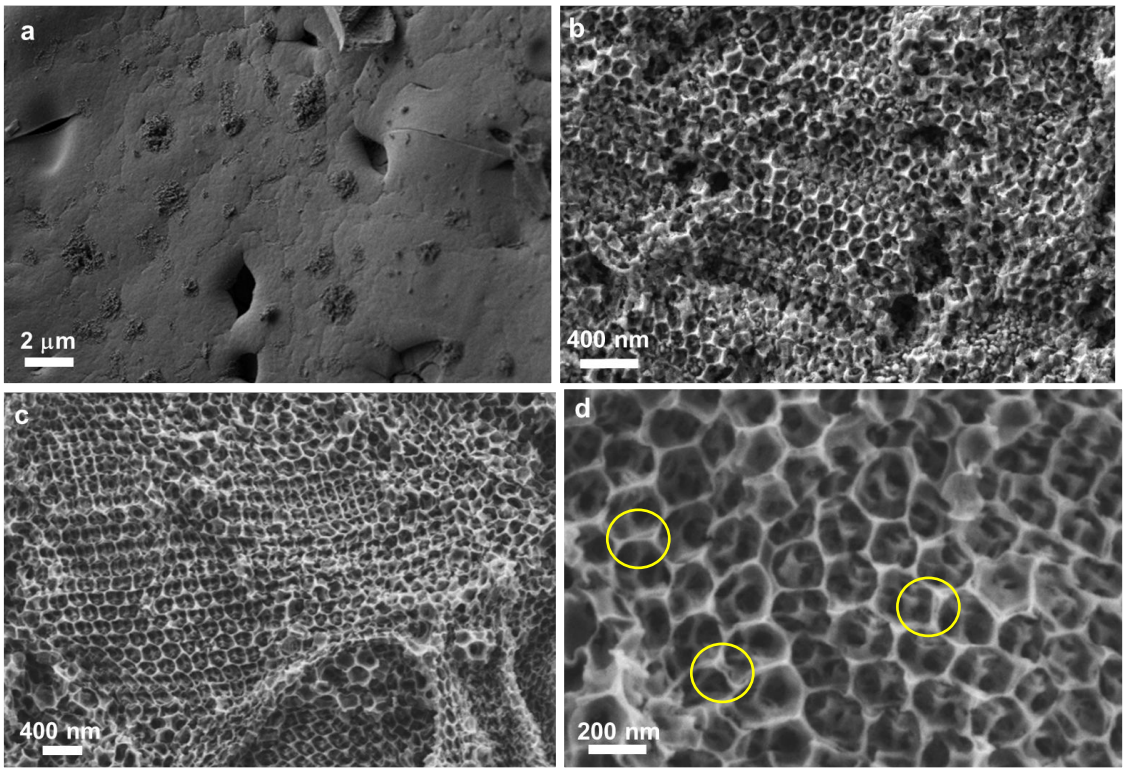

Figure 1. FESEM images of a) Ni/CeO_2-Ref, b) Ni/CeO_2-3DOM and c) and d) (Ni-Ce)-3DOM.

The incorporation of nickel to the PMMA template before cerium ((Ni-Ce)-3DOM catalyst; Figure 1d) improves the definition of the macrostructure with regard to Ni/CeO_2-3DOM. This fact can be explained taking into account the preparation method and the stability of the metal salts. To ensure the establishment of a 3DOM skeleton, the infiltrated and solidified precursor salt must have a higher melting point and a higher decomposition temperature than the PMMA template.[33] The melting point of cerium nitrate hexahydrate and nickel nitrate is 96 ºC [33] and 57 ºC,[34] respectively, which is lower than the glass transition temperature of PMMA template (around 115.9 ºC),[35] If an ethanol solution of cerium or nickel nitrate is used as direct precursor, the precursor nitrate would be separated from PMMA template due to its easy melting or be decomposed prior to the PMMA combustion and thus, to prejudice the formation of 3DOM structure. To preserve the 3DOM skeleton, cerium and nickel citrates are used as precursors. However, the

stability of these metal citrates is very different. The decomposition of cerium and nickel citrates occurs in the range of 263-300 ºC[36] and 335-350 ºC[37], respectively, whereas the combustion of PMMA template take place from 240 to 350 ºC.[36] Thus, the decomposition temperature of the cerium citrate overlaps, in part, the PMMA combustion and consequently, a slight collapse of the structure can be produced during the PMMA combustion in CeO_2-3DOM sample (**Figure 1b**). However, the decomposition of the nickel citrate occurs at higher temperatures in which most of the PMMA template has been removed. In this way, in (Ni-Ce)-3DOM sample the formation of a first layer of nickel citrate previous to the infiltration of a layer of cerium citrate make more stable the 3DOM structure and avoids the partial collapse observed for pure CeO_2-3DOM sample (**Figure 1c-d**).

These morphological differences are traduced to different textural properties. N_2 adsorption-desorption isotherms and pore size distributions determined by Hg-intrusion porosimetry are depicted in **Figure 2** and **3**, respectively. All samples show Type II -IV isotherms characteristics of non-porous or macroporous materials, however significant differences are observed between 3DOM and Ref catalysts. 3DOM samples are more porous materials than Ref one as denotes the higher N_2 uptake. Moreover, 3DOM samples present a well-defined hysteresis loop at high relative pressures characterized by a rapid increase of the slope at relative pressures close to 1, which suggests the presence of macropores. This loop is higher for (Ni-Ce)-3DOM sample due to the better-defined 3DOM structure observed by FESEM. A smaller hysteresis loop is observed at lower relative pressures in Ref samples denoting the presence of lower amount and narrower pores.

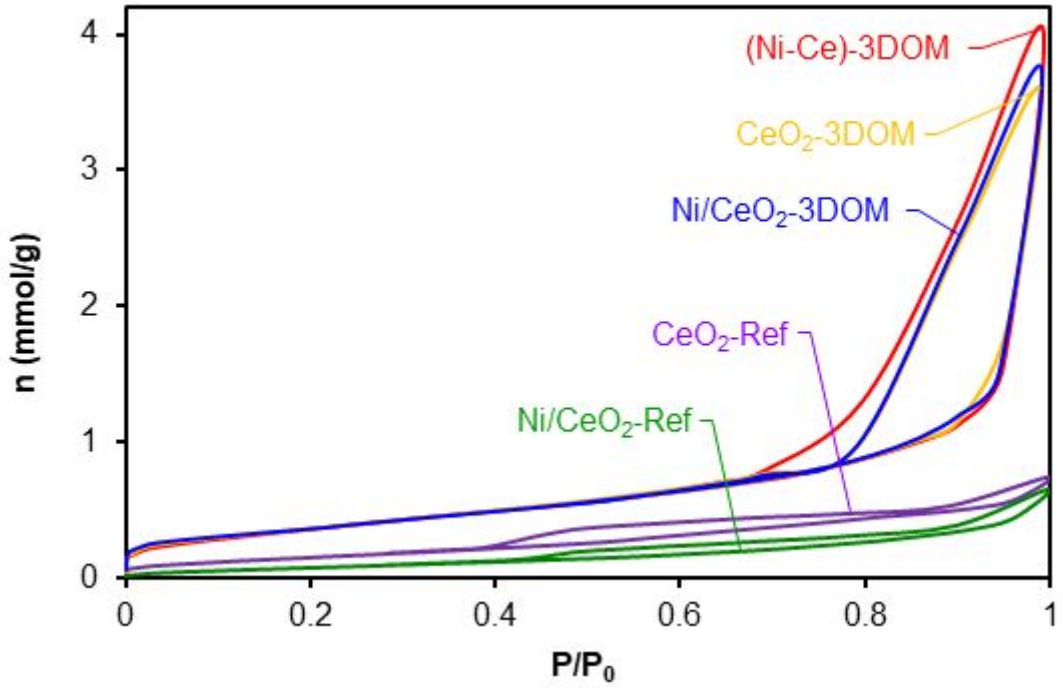

Figure 2. N_2 adsorption-desorption isotherms at -196ºC.

Comparing the textural properties of the supports and the Ni-containing catalysts, it is observed that the impregnation of Nickel to the CeO_2-Ref support produces a blockage of the microporosity and narrower mesoporosity, whereas no significant differences in porosity is observed between Ni/CeO_2-3DOM and CeO_2-3DOM samples (**Table 1**). This fact denotes that the surface area of the 3DOM support is high enough to disperse the nickel oxide particles without blocking the entrance to the pores measured by N_2 adsorption.

These observations were also corroborated by mercury intrusion porosimetry (**Figure 3**). A bimodal pore size distribution is obtained for all 3DOM catalysts in which two maxima are observed centred at pore radii of 40 and 90 nm, related to the interstitial spaces and to the porosity obtained by calcination of PMMA spheres, respectively, which perfectly match the pore size distribution observed by FESEM (**Figure S1)**. Moreover, according to N_2 adsorption-desorption isotherms, the (Ni-Ce)-3DOM catalyst is the one with the most developed meso and macroporosity ($V_{2\text{-}50}$ and $V_{50\text{-}800}$, **Table 1**).

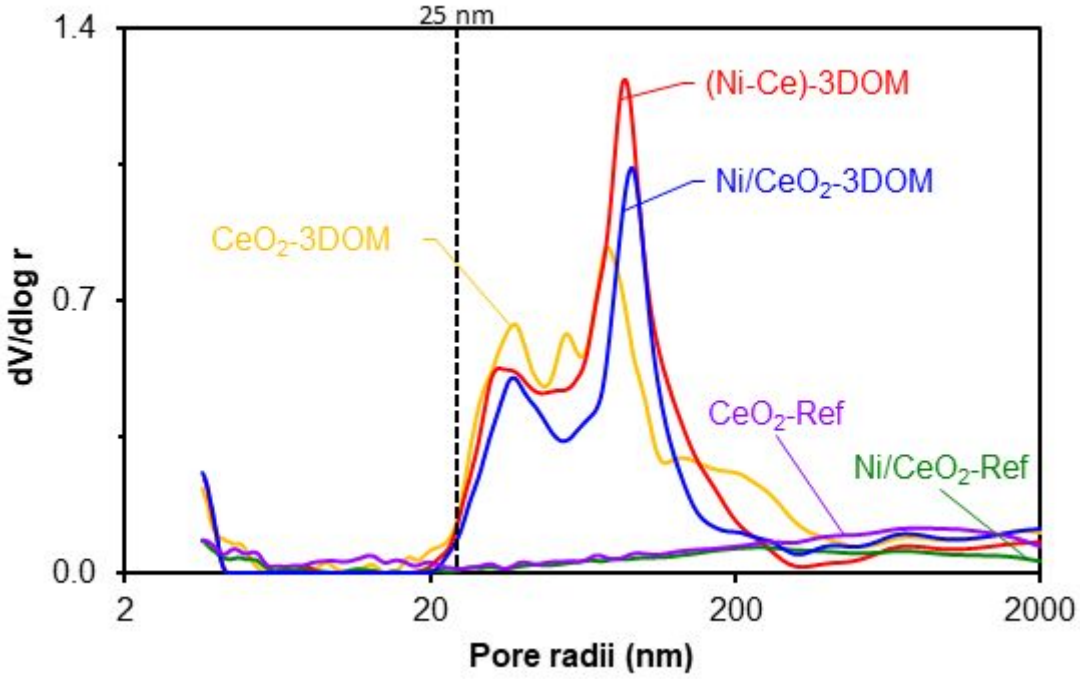

Figure 3. Pore size distributions determined by mercury intrusion porosimetry.

Table 1. Results of the catalysts characterization by N_2 adsorption, Hg porosimetry and XRD.

Muestra	$S_{B.E.T.}$ (m^2/g)	$V_{2\text{-}50\ nm}$ (cm^3/g)	$V_{50\text{-}800\ nm}$ (cm^3/g)	Cristallite size (nm)	Cell parameter (nm)
CeO_2-3DOM	32	0.13	0.34	14	0.5423
Ni/CeO_2-3DOM	31	0.12	0.31	15	0.5415
(Ni-Ce)-3DOM	35	0.15	0.38	8	0.5415
CeO_2-Ref	13	0.04	0.09	n.a.	n.a.
Ni/CeO_2-Ref	8	0.02	0.05	22	0.5423

3.2. Characterization of the crystallinity (XRD)

X-ray diffraction (XRD) was used to study the crystalline structure of the catalysts and diffractograms of all catalysts are shown in **Figure 4**. A cubic fluorite type crystal structure of CeO_2 phase (JCPDS 00-034-0394) is obtained for all catalysts. Note also that no insertion of nickel cations in the CeO_2 lattice is observed since the lattice parameters (**Table 1**) are very similar to each other and consistent with the value reported in the JCPDS database (0.5411 nm). Characteristic peaks of NiO (JCPDS 01-075-0269) are also

observed in the catalysts, and the intensity of those peaks depends on the Ni incorporation method employed. These peaks become wider and less intense in the case of (Ni-Ce)-3DOM denoting, as expected, a better dispersion of Ni nanoparticles along the ceria matrix when the nickel is added during the synthesis. Moreover, it is important to highlight the effect on the ceria crystallinity of the addition of nickel during the synthesis, (Ni-Ce)-3DOM, versus the introduction by impregnation after the support preparation, Ni/CeO_2-3DOM and Ni/CeO_2-Ref. The crystal size of ceria particles (**Table 1**) does not change if nickel is introduced by impregnation but decreases when the nickel is added during the synthesis. This suggests a sintering prevention of ceria particles during the subsequent calcination step which can be a consequence of the NiO-CeO_2 interaction, indicating a better and intimate contact in samples prepared by incorporation of Ni prior to the formation of the CeO_2 structure.

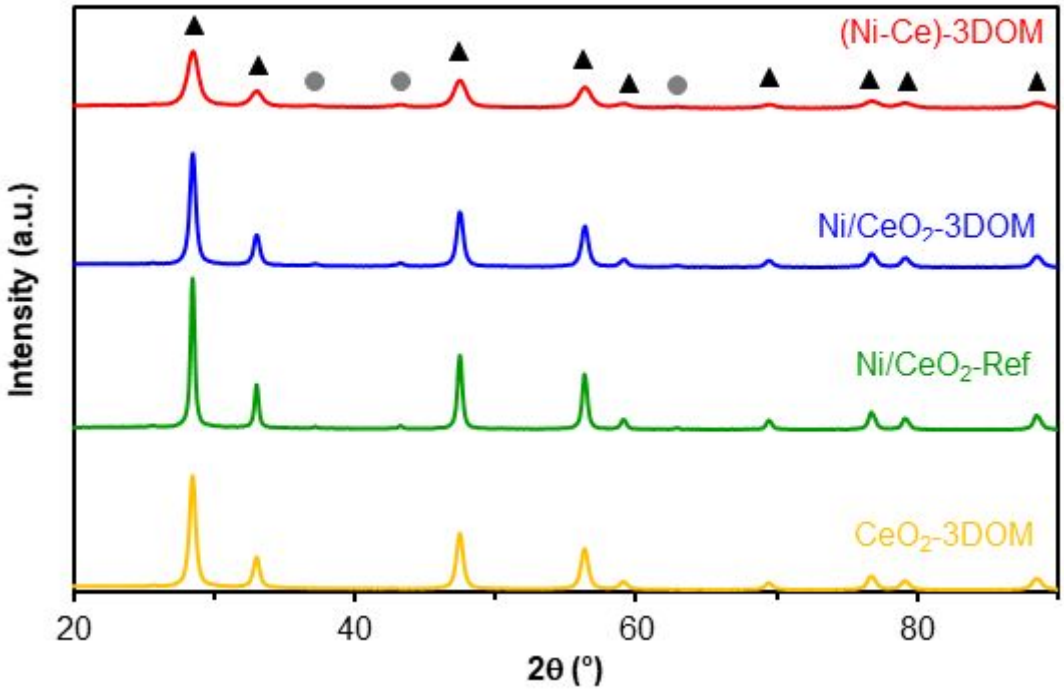

Figure 4. X-Ray diffractograms of the catalysts. Labeled peaks belong to CeO_2 (▲) and NiO (●) phases**.**

3.3. Characterization of the reducibility (H_2-TPR) and chemical surface.

The reducibility of the catalysts was studied by H_2-TPR experiments and results are depicted in **Figure 5**. Two peaks are observed at 560 ºC and 780 ºC in the H_2-TPR profile of CeO_2-3DOM support that can be attributed to the reduction of Ce^{4+} cations in the ceria surface and into the bulk, respectively. The reduction of bulk Ce^{4+} is also observed for CeO_2-Ref sample but surface reduction is not detected in this case which denoted an improved surface reducibility of the 3DOM structured catalysts. This improved reducibility of 3DOM structured samples is also pointed out in Ni/CeO_2 catalysts. Two TPR peaks can be usually observed in NiO/CeO_2 catalysts: a first weak TPR peak found around 250◦C might be ascribed to the reduction of very small NiO particles weakly interacting with ceria whereas a second sharp TPR peak observed at around 350 ºC is owing to the reduction of NiO particles and surface ceria.[38] Ni/CeO_2-Ref shows, in addition to the bulk Ce^{4+} reduction, a symmetrical reduction peak at 350 ºC corresponding to the reduction of Ni species. This peak is also observed in the Ni/CeO_2-3DOM catalyst, however a shoulder appears at 390 ºC toghether with a decrease of the surface ceria reduccion peak (560 ºC). Thus, this shoulder can be attributed to the Ni-catalized reduction of ceria surface which is favoured by the improved reducibility observed in 3DOM sample regarding Ref one. This Ni-catalized reduction of the ceria surface is also improved by the addition of the Ni precursor during the ceria synthesis, (Ni-Ce)-3DOM. The better dispersion of Ni-species and the improved Ce-Ni contact increases the Ni-catalized reduction of ceria and decreases the Ni^{2+} reduction peak, and consequently a broader reduction peak is obtained. Note also that the peak at 250 ºC ascribed to small NiO particles weakly interacting with ceria, only appears for Ni/CeO_2-Ref which denotes the lowest Ni-Ce interaction.

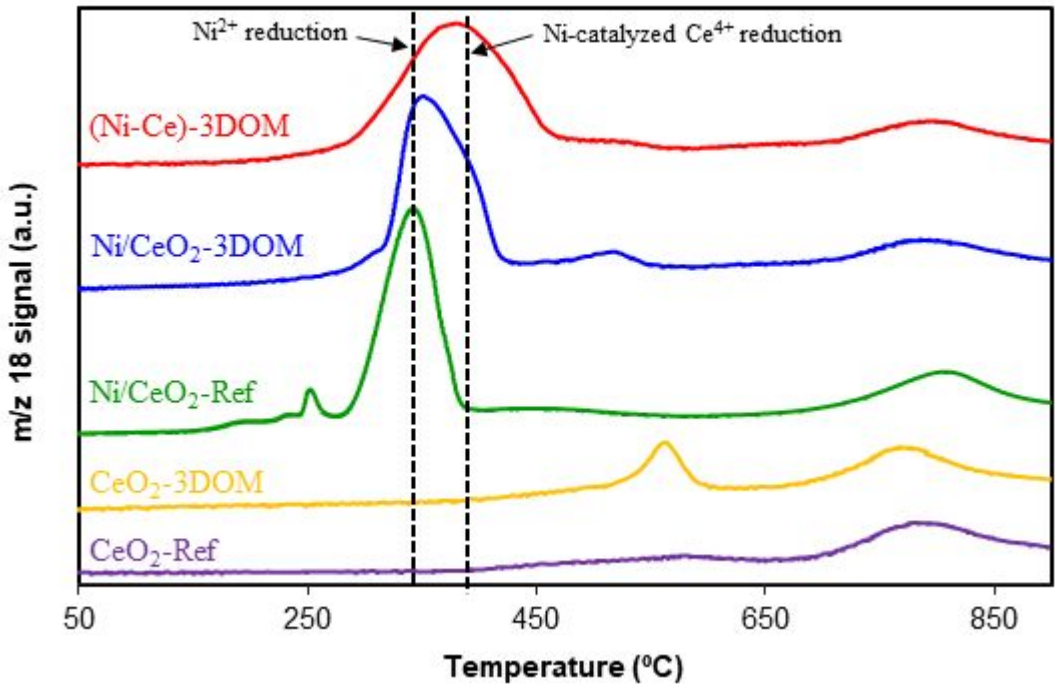

Figure 5. H_2-TPR characterization of the catalysts.

Quantitative calculations were performed using the area under the reduction peaks and a reference CuO sample and assuming the presence of Ni^{2+} in all cases. The consumption of H_2 obtained for Ni/CeO_2 ref is exactly the amount required for the 100 % reduction of Ni^{2+} to Ni^0. However, the consumption of H_2 is slightly higher (113 %) than the amount required to reduce all nickel on the Ni/CeO_2 3DOM catalyst, which evidences that Ce^{4+} cations are also reduced in this wide double peak. This H_2 consumption is 143 % for the sample (Ni-Ce)-3DOM corroborating the improved Ni-catalyzed reduction of surface ceria by the intimate Ni-Ce contact in this case.

These differences in the reducibility of ceria and Ni-Ce contact were also corroborated by the analysis of the surface chemistry of the catalysts by XPS. Ce3d, O1s and Ni2p XPS spectral regions are shown in **Figure 6**. 5 doublets are required to deconvolve the Ce3d region (**Figure 6a**). The peaks pairs at 882.0-900.3 eV, 888.2-907.0 eV, 898.0-916.3 are attributed to Ce^{4+} whereas the peaks at 880.3-898.6 eV and 884.0-902.3 eV are assigned to Ce^{3+}. The proportion of Ce^{3+} detected by XPS must be related

313 with the reducibility of the surface. As it was pointed out by H_2-TPR, the reducibility of
314 the surface is improved by the 3DOM structure and by the addition of Ni, mainly if this
315 Ni is incorporated during the synthesis due to the higher dispersion and Ce-Ni contact in
316 this case. Consequently, it is expected that the amount of Ce^{3+} detected by XPS follows
317 the same trend observed by H_2-TPR (**Figure 5**). Clearly, as it is observed from **Figure 6a**
318 and **Table 2**, the Ce^{3+} contents slightly increases in CeO_2-3DOM (22.2 %) regarding
319 CeO_2-Ref (19.9 %) due to the improved surface reducibility. This content is increased by
320 the addition of Ni, mainly in Ni/CeO_2-3DOM and (Ni-Ce)-3DOM due to the Ni-catalyzed
321 reduction of the CeO_2 surface observed.

322 This effect must be also observed in the O1s region. Two peaks are required to
323 deconvolute the O1s region of all catalysts (**Figure 6b**); one centered at 529.0 eV,
324 attributable to the surface lattice oxygen (O_{latt}) and another one centered at 531.0 eV,
325 assigned to adsorbed oxygen species (O_{ads}, e.g. O^-, O_2^{2-} or O_2^-). The O_{ads} species are
326 usually present at the oxygen vacancies and thus, a large amount of O_{ads} species implies
327 a higher oxygen vacancy population. Consequently, the surface O_{ads}/O_{latt} ratio can be also
328 indicative of the surface reducibility. O_{ads}/O_{latt} ratios of the prepared catalysts are
329 collected in **Table 2.** The trend observed is CeO_2-Ref < Ni/CeO_2-Ref < CeO_2-3DOM<
330 Ni/CeO_2-3DOM < (Ni-Ce)-3DOM which perfectly match the trend in the improvement
331 of reducibility observed by H_2-TPR.

332 $Ni2p_{3/2}$ core level spectra as well as the relative contribution of each peak are
333 depicted in **Figure 6c**. The $Ni2p_{3/2}$ spectral region shows a main band in the range 851–
334 859 eV together with a satellite structure at higher BE (859-866 eV). The assignment of
335 Ni_{2p} peaks is still a matter of debate, but it has been proposed that the nature of the nickel
336 species can be inferred from the peaks of greater intensity.[39,40] According to literature,
337 the main peaks centred at 852.3, 853.4 and 856.7 eV can be assigned to metallic Ni, NiO,

and Ni_2O_3, respectively.[39,41–43],. The peak at 856.0 eV can be also attributed to surface Ni^{3+} species associated to the presence of Ni^{2+} vacancies in NiO crystal lattices[41] which is close to the binding energy of Ni_2O_3 and $Ni(OH)_2$.[44] The peaks centred at 861.2 eV corresponds to satellites attributed to Ni in the form of oxide and hydroxide phases.[45] In our case, three peaks are required to deconvolve the $Ni2p_{3/2}$ region at around 853.2, 855.0 and 857.2 eV, which can be assigned to surface Ni^{2+} species in NiO structure (surface NiO species), Ni^{2+} species in intimate contact with ceria surface (NiO-Ce species)[44] and Ni^{3+} or $Ni(OH)_2$ species, respectively. Consequently, the different Ni-Ce interaction can be analysed considering the relative proportion of each peak (**Figure 6c**). It can be observed that the proportion of each active site depends on the Ni incorporation method. Catalysts prepared by impregnation (Ni/CeO_2 3DOM and Ni/CeO_2-Ref) present the highest proportion of surface NiO species and, therefore, the least amount of NiO in intimate contact. This percentage of surface NiO species decreases if Ni is incorporated prior to the 3DOM formation at the expense of an increase of the Ni^{2+} species in intimate contact (NiO-Ce) denoting the greatest contact between ceria and Ni phases.

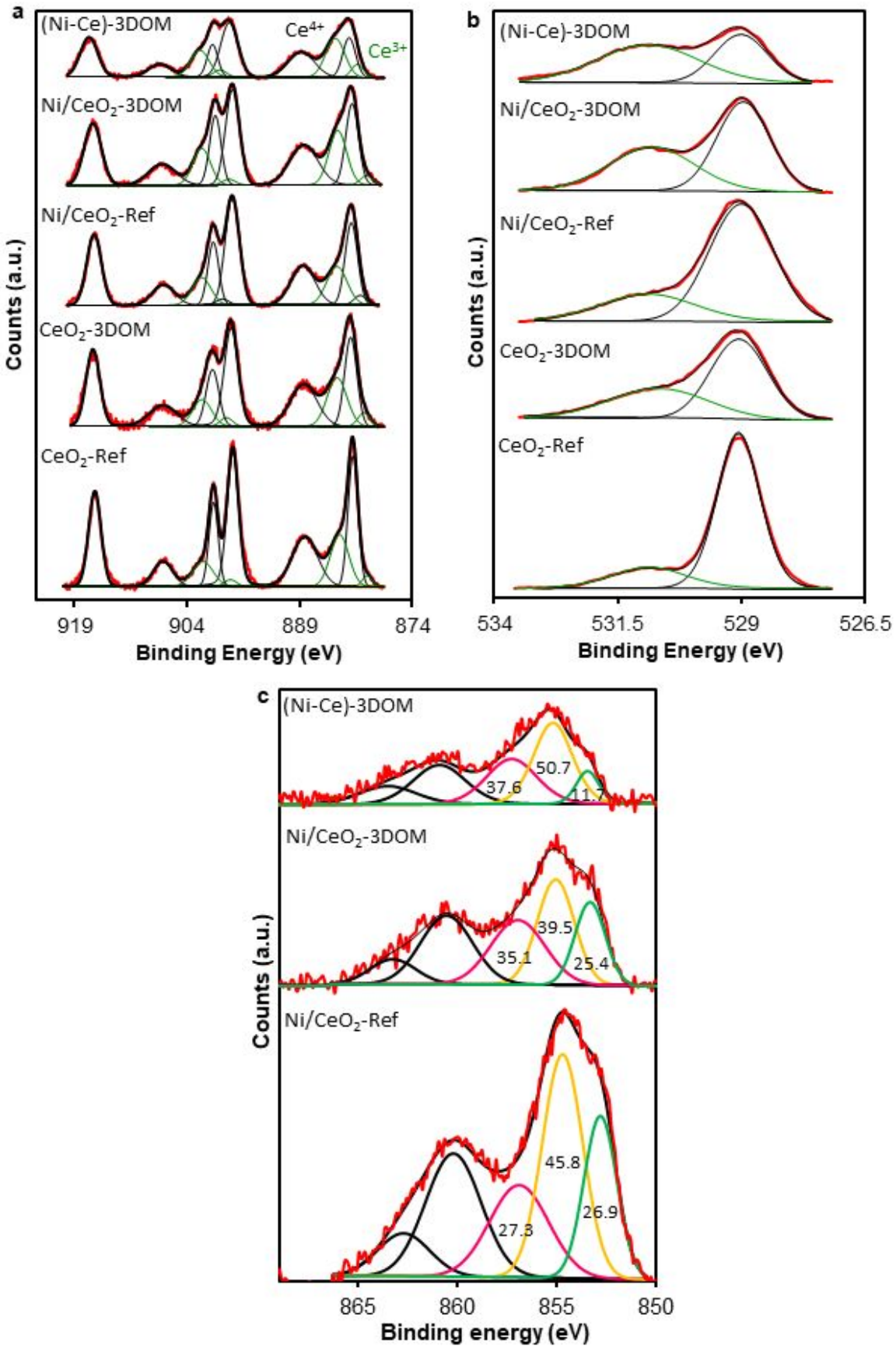

Figure 6. XPS results: a) Ce3d, b) O1s and c) $Ni2p_{3/2}$ of catalysts

Tabla 2. Surface composition of catalysts determined by XPS and total Ni content determined by ICP-OES (data in wt. %)

	ICP-OES	XPS					
Catalyst	**Ni**	**C**	**O**	**Ni**	**Ce**	**Ce^{3+}**	**O_{ads}/O_{latt}**
CeO_2-Ref	-	14.0	18.9	0.0	67.1	19.9	0.23
CeO_2 3DOM	-	9.6	20.7	0.0	69.8	22.2	0.62
Ni/CeO_2-Ref	8.8	8.0	22.7	17.4	52.7	20.5	0.32
Ni/CeO_2-3DOM	10.4	10.6	20.8	8.8	59.9	23.2	0.81
(Ni-Ce)-3DOM	8.3	13.6	22.3	7.9	56.2	37.4	1.50

The Ni dispersion and, indirectly, the Ni-Ce contact is also reflected by the amount of Ni on the catalysts surface (**Table 2**). It can be observed that the dispersion obtained also depends on the Ni-incorporation method. The real percentage of Ni incorporated in the catalysts (Ni_{ICP}) is very similar for all catalysts, and very closed to the theoretical value (around 8.5 %), which allows easy comparison of the catalytic results. However, Ni_{XPS} contents are closed to real values (Ni_{ICP}) in (Ni-Ce)-3DOM and Ni/CeO_2-3DOM catalysts, which manifests a high dispersion of Ni particles along the ceria matrix, as it was also confirmed by XRD due to a high distribution of Ni precursor during the synthesis or the Ni dispersion inside the porosity (macroporosity) of the CeO_2-3DOM support. Nonetheless, Ni_{XPS} content is higher than the real value (Ni_{ICP}) for impregnated Ref sample (Ni/CeO_2-Ref), denoting accumulation of Ni on the external surface of ceria. As consequence of this better dispersion and Ni-Ce contact, the reducibility of these samples is improved regarding Ni/CeO_2-Ref samples, as it was pointed out above.

3.4. Catalytic oxidation of soot in presence of O_2 and NO_x

In presence of NO_x and O_2, the catalytic combustion of soot can occur by two different mechanisms: the active oxygen or the NO_2-assisted mechanisms. In the former, the most effective one, a good solid-solid contact is required for an efficient active oxygen transfer from the catalyst surface to the soot, whereas in the latter, an improved catalytic oxidation of NO to NO_2 is mandatory. In any case, the generation of active oxygen is a

386 key factor to improve the catalytic soot combustion activity. Consequently, the improved
387 reducibility observed by XPS and H_2-TPR and the 3DOM structure are expected to
388 influence the catalytic combustion of soot.

389 As commented, the Ni incorporation method and the 3DOM structure affect to the
390 Ni dispersion and Ni-Ce contact which clearly influences the reducibility and the active
391 oxygen generation (O_{ads}/O_{latt}, **Table 2**). Thus, differences in the catalytic oxidation of NO
392 to NO_2 must be observed between all the prepared catalysts. NO_2 profiles in catalytic NO-
393 oxidation experiments in absence of soot are depicted in **Figure 7**. NO_2 profiles increase
394 with temperature until a maximum where thermodynamic equilibrium is achieved, and
395 above that temperature the NO_2 profiles decrease following thermodynamics. The NO_2
396 production is related with the reducibility and the active oxygen generation (O_{ads}/O_{latt})
397 observed by XPS. CeO_2-Ref is the catalysts with the lowest ability to oxidize NO to NO_2
398 due to their limited generation of active oxygen. This active oxygen generation is
399 improved by the 3DOM structure and by the incorporation of Ni and consequently, an
400 increase of the NO_2 generation is observed for Ni-based and 3DOM structured catalysts.
401 It is also important to highlight, that the incorporation of Ni during the synthesis improved
402 in a high extent the active oxygen generation due to the improved Ni-Ce contact and thus,
403 (Ni-Ce)-3DOM is the sample which presents the highest ability to oxidize NO to NO_2.

404

405

406

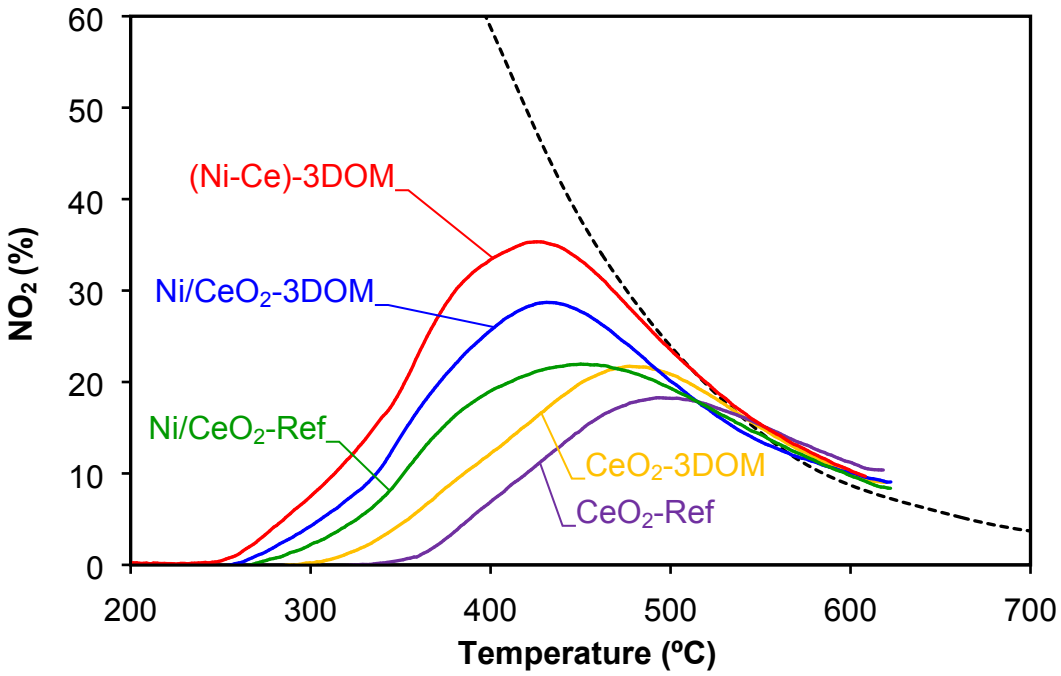

Figure 7. NO_2 profiles in catalytic experiments performed without soot

This improved generation of active oxygen and NO_2 production by the introduction of Ni and the 3DOM structure affects the soot combustion activity. This is confirmed in the catalytic soot combustion experiments performed with O_2+NO. CO_x evolution profiles and the CO_2 selectivity values are shown in **Figure 8** and **Table 3**, respectively. All catalysts decrease the soot combustion temperature and increase the CO_2 selectivity regarding the uncatalyzed reaction, however both activity and selectivity depends on both the catalyst composition and morphology.

As it was previously pointed out, two mechanisms are acting in presence of NO and O_2, and thus two factors must be considered i) the generation of active oxygen and NO_2 generation and ii) the transfer of this active oxygen from the catalysts to the soot. In 3DOM samples both factors are improved and thus, these samples are more active and selective than Ref ones. In addition, the incorporation of Ni improves the generation of active oxygen and therefore, Ni-containing catalyst are more active and selective than pure supports. However, despite Ni/CeO_2-Ref generates more NO_2 than CeO_2-3DOM, is

423 less active, indicating that the active-oxygen mechanism is the main pathway and the
424 produced NO_2, which is much more oxidising than O_2 and NO, interacts with the catalyst
425 to create more active oxygen,[46] this is, NO_2 is a strong oxidising agent and it is postulated
426 that NO_2 is able to transfer its oxygen to the catalyst surface.[47] This was also pointed out
427 analysing the NO_2 profiles in presence of soot. NO_2 profiles for impregnated Ref and
428 3DOM samples (Ni/CeO_2-Ref and Ni/CeO_2-3DOM) with and without soot are compared
429 in **Figure S2**. In both catalysts, the generated NO_2 directly or indirectly reacts with soot,
430 however, the amount of NO_2 reacted using Ni/CeO_2-3DOM is higher than using Ni/CeO_2-
431 Ref. This manifest that the NO_2 reaction with soot is more efficient in 3DOM structured
432 samples and thus, the most significant pathway is the NO_2 interaction with the catalyst to
433 create more active oxygen to be transferred to the soot. Therefore, the 3DOM structure is
434 very important to really improve the catalytic activity. It is also important to identify the
435 NO_x reduction by soot and thus, the NO_x profiles have been included in **Figure S2b**.
436 There are not evidences of NO_x removal/chemisorption from the gas stream on the
437 catalysts during the catalytic experiments performed without soot in the 200-700 ^{0}C range.
438 However, in presence of soot, NO_x profiles obtained show a minimum which matches the
439 soot combustion temperature range of each sample and thus must be attributed to NO_x
440 reduction by soot, which occurs together with soot gasification. Similar NOx reduction is
441 detected for all catalysts (around 8 %) and consequently, a similar interaction of NO_x with
442 soot could be deduced.

443

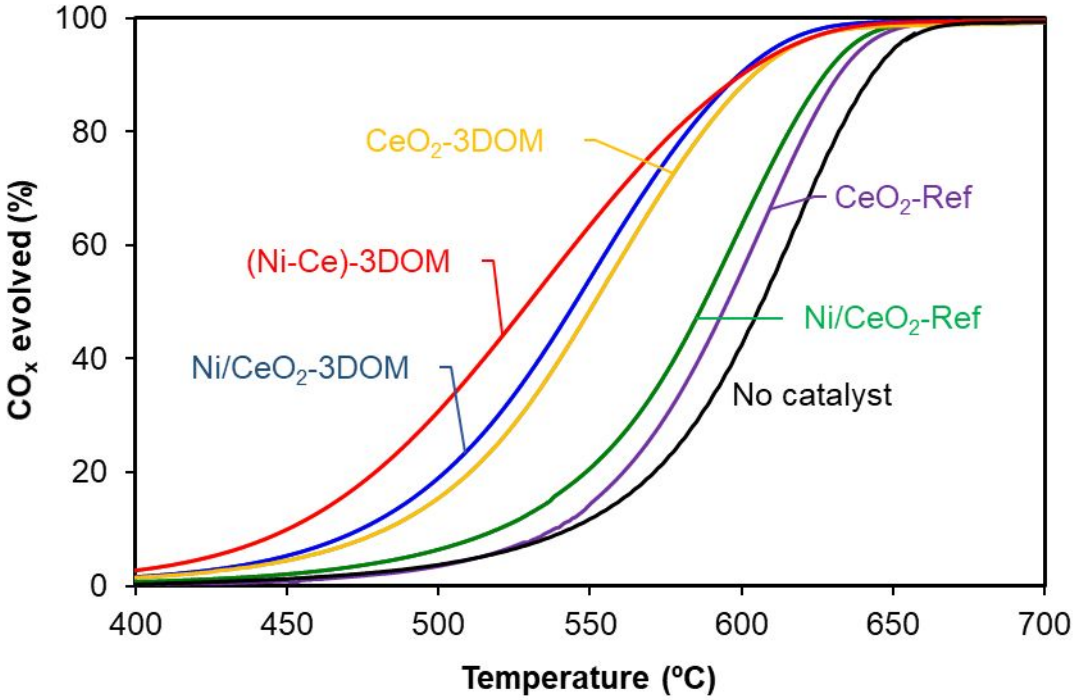

Figure 8. Soot combustion experiments in presence of 500 ppm NO and 5% O_2 in N_2.

Table 3. Selectivity to CO_2 (S_{CO_2}) and Temperature required to achieve the 50% (T50) and 100% (T100) of conversion in soot combustion experiments

Sample	S_{CO_2} (%)	T50	T100
No Catalysts	33.2	608.0	661.5
CeO_2-Ref	68.9	595.3	650.5
CeO_2-3DOM	84.2	551.6	634.0
Ni/CeO_2-Ref	86.7	587.8	645.8
Ni/CeO_2-3DOM	96.6	545.3	624.9
(Ni-Ce)-3DOM	98.2	530.2	632.2

Finally, remark that the combination of an optimal Ni-Ce contact (by the addition of Ni precursors during the synthesis) with a 3DOM structure is an excellent strategia to produce catalysts with improved performance for the catalytic combustion of soot.

4. CONCLUSIONS

The effect of Ni-doping of CeO_2 and the 3DOM structure on the physicochemical properties and catalytic activity for the soot combustion was studied. Moreover, the Ni-incorporation method to the ceria support was also investigated. Thus, Ni/CeO_2 catalysts

were obtained with uncontrolled (Ref) and 3DOM structured morphology and the Ni incorporated before or during the synthesis of the CeO_2 support. The main conclusions reached are summarized below:

- The 3DOM structure improves the soot combustion since the catalysts have a higher surface area and an adequate pore size for the catalytic oxidation of soot. This structure allows to improve the contact between the soot and the catalyst particles. Consequently, by increasing the contact points, the catalytic performance is improved, and the soot is oxidized at a lower temperature than using a catalyst without a defined structure.
- Doping CeO_2 with Ni improves the soot combustion catalytic activity. This is because NiO improves the catalytic oxidation of NO to NO_2. From the XPS results it has been concluded that the doping of CeO_2 with Ni also improves the production of active oxygen and the oxygen storage capacity of the catalyst.
- It has been shown that the way in which Ni is introduced into the catalyst affects its physicochemical and catalytic properties. By introducing the Ni by successive infiltration into the solid template (Ni-Ce 3DOM) the size of the crystals is decreased, the dispersion of the nickel in the catalyst is improved, and the reducibility is enhanced regarding the impregnated catalyst (Ni/CeO_2-3DOM). As results, the Ni-Ce 3DOM catalyst is the one that most decreases the soot combustion temperature.

5. ASSOCIATED CONTENT

*Supporting Information

The Supporting Information is available online.

Pore size distribution of (Ni-Ce)-3DOM obtained from the analysis of FESEM images; NO_2 and NO_x profiles in catalytic experiments performed with and without soot for impregnated Ref and 3DOM samples.

6. ACKNOWLEDGEMENTS

The authors thank the financial support of the Spanish Ministry of Economy and Competitiveness (Project CTQ2015-67597-C2-2-R and grant FJCI-2015-23769), the Spanish Ministry of Education, Culture and Sports (grant FPU14/01178), Generalitat Valenciana (Project PROMETEO/2018/076) and the UE (FEDER funding).

7. REFERENCES

(1) MacIel, C. G.; Silva, T. D. F.; Hirooka, M. I.; Belgacem, M. N.; Assaf, J. M. Effect of Nature of Ceria Support in CuO/CeO_2 Catalyst for PROX-CO Reaction. *Fuel* **2012**, *97*, 245–252.

(2) Diwell, A. F.; Rajaram, R. R.; Shaw, H. A.; Truex, T. J. The Role of Ceria in Three-Way Catalysts. *Stud. Surf. Sci. Catal.* **1991**, *71* (C), 139–152.

(3) Zhao, M.; Chen, S.; Zhang, X.; Gong, M.; Chen, Y. Performance of Pd/CeO_2-$_{ZrO2}$-Al_2O_3 Catalyst for Motorcycle. *J. Rare Earths* **2009**, *27* (5), 728–732.

(4) Liu, S.; Wu, X.; Weng, D.; Ran, R. Ceria-Based Catalysts for Soot Oxidation: A Review. *J. Rare Earths* **2015**, *33* (6), 567–590.

(5) Bueno-López, A. Diesel Soot Combustion Ceria Catalysts. *Appl. Catal. B Environ.* **2014**, *146*, 1–11.

(6) Piumetti, M.; Andana, T.; Bensaid, S.; Fino, D.; Russo, N.; Pirone, R. Ceria-Based Nanomaterials as Catalysts for CO Oxidation and Soot Combustion: Effect of Zr-Pr Doping and Structural Properties on the Catalytic Activity. *AIChE J.* **2017**, *63* (1), 216–225.

(7) Nascimento, L. F.; Martins, R. F.; Silva, R. F.; De Sousa Filho, P. C.; Serra, O. A. Ru-Doped Ceria-Zirconia Mixed Oxides Catalyze Soot Combustion. *React. Kinet. Mech. Catal.* **2014**, *111* (1), 149–165.

(8) Katta, L.; Sudarsanam, P.; Thrimurthulu, G.; Reddy, B. M. Doped Nanosized Ceria Solid Solutions for Low Temperature Soot Oxidation: Zirconium versus

Lanthanum Promoters. *Appl. Catal. B Environ.* **2010**, *101* (1–2), 101–108.

(9) Harada, K.; Oishi, T.; Hamamoto, S.; Ishihara, T. Lattice Oxygen Activity in Pr- and La-Doped CeO_2 for Low-Temperature Soot Oxidation. *J. Phys. Chem. C* **2014**, *118* (1), 559–568.

(10) Guillén-Hurtado, N.; García-García, A.; Bueno-López, A. Active Oxygen by Ce-Pr Mixed Oxide Nanoparticles Outperform Diesel Soot Combustion Pt Catalysts. *Appl. Catal. B Environ.* **2015**, *174–175* (2), 60–66.

(11) Andana, T.; Piumetti, M.; Bensaid, S.; Russo, N.; Fino, D.; Pirone, R. Nanostructured Ceria-Praseodymia Catalysts for Diesel Soot Combustion. *Appl. Catal. B Environ.* **2016**, *197*, 125–137.

(12) Małecka, M. A.; Kepiński, L.; Miśta, W. Structure Evolution of Nanocrystalline CeO_2 and $CeLnO_x$ Mixed Oxides (Ln = Pr, Tb, Lu) in O_2 and H_2 Atmosphere and Their Catalytic Activity in Soot Combustion. *Appl. Catal. B Environ.* **2007**, *74* (3–4), 290–298.

(13) Liu, J.; Zhao, Z.; Xu, C.; Liu, J. Structure, Synthesis, and Catalytic Properties of Nanosize Cerium-Zirconium-Based Solid Solutions in Environmental Catalysis. *Chinese J. Catal.* **2019**, *40* (10), 1438–1487.

(14) Huang, H.; Liu, J.; Sun, P.; Ye, S.; Liu, B. Effects of Mn-Doped Ceria Oxygen-Storage Material on Oxidation Activity of Diesel Soot. *RSC Adv.* **2017**, *7* (12), 7406–7412.

(15) Laguna, O. H.; Centeno, M. A.; Boutonnet, M.; Odriozola, J. A. Fe-Doped Ceria Solids Synthesized by the Microemulsion Method for CO Oxidation Reactions. *Appl. Catal. B Environ.* **2011**, *106* (3–4), 621–629.

(16) Zhu, H.; Xu, J.; Yichuan, Y.; Wang, Z.; Gao, Y.; Liu, W.; Yin, H. Catalytic Oxidation of Soot on Mesoporous Ceria-Based Mixed Oxides with Cetyltrimethyl Ammonium Bromide (CTAB)-Assisted Synthesis. *J. Colloid Interface Sci.* **2017**, *508*, 1–13.

(17) Aneggi, E.; de Leitenburg, C.; Dolcetti, G.; Trovarelli, A. Diesel Soot Combustion

Activity of Ceria Promoted with Alkali Metals. *Catal. Today* **2008**, *136* (1–2), 3–10.

(18) Castoldi, L.; Matarrese, R.; Lietti, L.; Forzatti, P. Intrinsic Reactivity of Alkaline and Alkaline-Earth Metal Oxide Catalysts for Oxidation of Soot. *Appl. Catal. B Environ.* **2009**, *90* (1–2), 278–285.

(19) Lim, C. B.; Kusaba, H.; Einaga, H.; Teraoka, Y. Catalytic Performance of Supported Precious Metal Catalysts for the Combustion of Diesel Particulate Matter. *Catal. Today* **2011**, *175* (1), 106–111.

(20) Aouad, S.; Abi-Aad, E.; Aboukaïs, A. Simultaneous Oxidation of Carbon Black and Volatile Organic Compounds over Ru/CeO_2 Catalysts. *Appl. Catal. B Environ.* **2009**, *88* (3–4), 249–256.

(21) Xiong, J.; Wu, Q.; Mei, X.; Liu, J.; Wei, Y.; Zhao, Z.; Wu, D.; Li, J. Fabrication of Spinel-Type $Pd_xCo_{3-X}O_4$ Binary Active Sites on 3D Ordered Meso-Macroporous Ce-Zr-O_2 with Enhanced Activity for Catalytic Soot Oxidation. *ACS Catal.* **2018**, *8* (9), 7915–7930.

(22) Xiong, J.; Mei, X.; Liu, J.; Wei, Y.; Zhao, Z.; Xie, Z.; Li, J. Efficiently Multifunctional Catalysts of 3D Ordered Meso-Macroporous $Ce_{0.3}Zr_{0.7}O_2$-Supported PdAu@CeO_2 Core-Shell Nanoparticles for Soot Oxidation: Synergetic Effect of Pd-Au-CeO_2 Ternary Components. *Appl. Catal. B Environ.* **2019**, *251* (December 2018), 247–260.

(23) Jin, B.; Wei, Y.; Zhao, Z.; Liu, J.; Jiang, G.; Duan, A. Effects of Au-Ce Strong Interactions on Catalytic Activity of Au/CeO_2/3DOM Al_2O_3 Catalyst for Soot Combustion under Loose Contact Conditions. *Cuihua Xuebao/Chinese J. Catal.* **2016**, *37* (6), 923–933.

(24) Liu, J.; Liu, J. Pyrolysis of Heavy Oil in the Presence of Supercritical Water: The Reaction Kinetics in Different Phases. *AICHE J.* **2015**, *61* (3), 857–866.

(25) Wang, J.; Cheng, L.; An, W.; Xu, J.; Men, Y. Boosting Soot Combustion Efficiencies over CuO-CeO_2 Catalysts with a 3DOM Structure. *Catal. Sci. Technol.* **2016**, *6* (19), 7342–7350.

564 (26) Alcalde-Santiago, V.; Bailón-García, E.; Davó-Quiñonero, A.; Lozano-Castelló,
565 D.; Bueno-López, A. Three-Dimensionally Ordered Macroporous PrOx: An
566 Improved Alternative to Soot Combustion Ceria Catalysts. *Appl. Catal. B Environ.*
567 **2018**, *In press* (July), 6.

568 (27) Wang, J.; Cheng, L.; An, W.; Xu, J.; Men, Y. Boosting Soot Combustion
569 Efficiencies over CuO-CeO_2 Catalysts with a 3DOM Structure. *Catal. Sci. Technol.*
570 **2016**, *6* (19), 7342–7350.

571 (28) Wu, Q.; Jing, M.; Wei, Y.; Zhao, Z.; Zhang, X.; Xiong, J.; Liu, J.; Song, W.; Li, J.
572 High-Efficient Catalysts of Core-Shell Structured Pt@transition Metal Oxides
573 (TMOs) Supported on 3DOM-Al_2O_3 for Soot Oxidation: The Effect of Strong Pt-
574 TMO Interaction. *Appl. Catal. B Environ.* **2019**, *244* (November 2018), 628–640.

575 (29) Wu, Q.; Xiong, J.; Zhang, Y.; Mei, X.; Wei, Y.; Zhao, Z.; Liu, J.; Li, J. Interaction-
576 Induced Self-Assembly of Au@La_2O_3 Core-Shell Nanoparticles on $La_2O_2CO_3$
577 Nanorods with Enhanced Catalytic Activity and Stability for Soot Oxidation. *ACS*
578 *Catal.* **2019**, *9* (4), 3700–3715.

579 (30) Alcalde-Santiago, V.; Davó-Quiñonero, A.; Lozano-Castelló, D.; Bueno-López, A.
580 On the Soot Combustion Mechanism Using 3DOM Ceria Catalysts. *Appl. Catal.*
581 *B Environ.* **2018**, *234* (April), 187–197.

582 (31) Burton, A. W.; Ong, K.; Rea, T.; Chan, I. Y. On the Estimation of Average
583 Crystallite Size of Zeolites from the Scherrer Equation: A Critical Evaluation of
584 Its Application to Zeolites with One-Dimensional Pore Systems. *Microporous*
585 *Mesoporous Mater.* **2009**, *117* (1–2), 75–90.

586 (32) Scherrer, P. Bestimmung Der Größe Und Der Inneren Struktur von Kolloidteilchen
587 Mittels Röntgenstrahlen. *Göttinger Nachrichten Math. Phys* **1918**, *2*, 98–100.

588 (33) Li, S.; Zheng, J.; Yang, W.; Zhao, Y.; Liu, Y. Preparation and Characterization of
589 Three-Dimensional Ordered Macroporous Rare Earth Oxide-CeO_2. *J. Porous*
590 *Mater.* **2008**, *15* (5), 589–592.

591 (34) Brockner, W.; Ehrhardt, C.; Gjikaj, M. Thermal Decomposition of Nickel Nitrate
592 Hexahydrate, $Ni(NO_3)_2 \cdot 6H_2O$, in Comparison to $Co(NO_3)_2 \cdot 6H_2O$ and

593 $Ca(NO_3)_2 \cdot 4H_2O$. *Thermochim. Acta* **2007**, *456* (1), 64–68.

594 (35) Berrahou, N.; Mokaddem, A.; Doumi, B.; Hiadsi, S.; Beldjoudi, N.; Boutaous, A.
595 Investigation by Molecular Dynamics Simulation of the Glass Transition
596 Temperature and Elastic Properties of Amorphous Polymers PMMA, PMAAM
597 and PMMA Co PMAAM Copolymers. *Polym. Bull.* **2016**, *73* (11), 3007–3017.

598 (36) Davó-Quiñonero, A.; González-Mira, J.; Lozano-Castelló, D.; Bueno-López, A.
599 Templated Synthesis of Pr-Doped Ceria with Improved Micro and Mesoporosity
600 Porosity, Redox Properties and Catalytic Activity. *Catal. Letters* **2018**, *148* (1),
601 258–266.

602 (37) He, S.; Zheng, X.; Mo, L.; Yu, W.; Wang, H.; Luo, Y. Characterization and
603 Catalytic Properties of Ni/SiO_2 Catalysts Prepared with Nickel Citrate as Precursor.
604 *Mater. Res. Bull.* **2014**, *49* (1), 108–113.

605 (38) Le, T. A.; Kim, M. S.; Lee, S. H.; Kim, T. W.; Park, E. D. CO and CO_2 Methanation
606 over Supported Ni Catalysts. *Catal. Today* **2017**, *293–294*, 89–96.

607 (39) Grosvenor, A. P.; Biesinger, M. C.; Smart, R. S. C.; McIntyre, N. S. New
608 Interpretations of XPS Spectra of Nickel Metal and Oxides. *Surf. Sci.* **2006**, *600*
609 (9), 1771–1779.

610 (40) Marrani, A. G.; Novelli, V.; Sheehan, S.; Dowling, D. P.; Dini, D. Probing the
611 Redox States at the Surface of Electroactive Nanoporous Nio Thin Films. *ACS*
612 *Appl. Mater. Interfaces* **2014**, *6* (1), 143–152.

613 (41) Xu, X.; Li, L.; Yu, F.; Peng, H.; Fang, X.; Wang, X. Mesoporous High Surface
614 Area NiO Synthesized with Soft Templates: Remarkable for Catalytic CH_4 Deep
615 Oxidation. *Mol. Catal.* **2017**, *441* (February 2018), 81–91.

616 (42) Yu, G. H.; Zeng, L. R.; Zhu, F. W.; Chai, C. L.; Lai, W. Y. Magnetic Properties
617 and X-Ray Photoelectron Spectroscopy Study of NiO/NiFe Films Prepared by
618 Magnetron Sputtering. *J. Appl. Phys.* **2001**, *90* (8), 4039–4043.

619 (43) Ahmed, A.; Ali, T.; Naseem Siddique, M.; Ahmad, A.; Tripathi, P. Enhanced
620 Room Temperature Ferromagnetism in Ni Doped SnO_2 Nanoparticles: A

621 Comprehensive Study. *J. Appl. Phys.* **2017**, *122* (8).

622 (44) Weidler, N.; Schuch, J.; Knaus, F.; Stenner, P.; Hoch, S.; Maljusch, A.; Schäfer,
623 R.; Kaiser, B.; Jaegermann, W. X-Ray Photoelectron Spectroscopic Investigation
624 of Plasma-Enhanced Chemical Vapor Deposited NiO_x, $NiO_x(OH)_y$, and
625 $CoNiO_x(OH)_y$: Influence of the Chemical Composition on the Catalytic Activity
626 for the Oxygen Evolution Reaction. *J. Phys. Chem. C* **2017**, *121* (12), 6455–6463.

627 (45) Hengne, A. M.; Samal, A. K.; Enakonda, L. R.; Harb, M.; Gevers, L. E.; Anjum,
628 D. H.; Hedhili, M. N.; Saih, Y.; Huang, K. W.; Basset, J. M. Ni-Sn-Supported ZrO_2
629 Catalysts Modified by Indium for Selective CO_2 Hydrogenation to Methanol. *ACS*
630 *Omega* **2018**, *3* (4), 3688–3701.

631 (46) Atribak, I.; López-Suárez, F. E.; Bueno-López, A.; García-García, A. New Insights
632 into the Performance of Ceria-Zirconia Mixed Oxides as Soot Combustion
633 Catalysts. Identification of the Role of "Active Oxygen" Production. *Catal. Today*
634 **2011**, *176* (1), 404–408.

635 (47) Setiabudi, A.; Chen, J.; Mul, G.; Makkee, M.; Moulijn, J. A. CeO_2 Catalysed Soot
636 Oxidation: The Role of Active Oxygen to Accelerate the Oxidation Conversion.
637 *Appl. Catal. B Environ.* **2004**, *51* (1), 9–19.

638